Rare Metal Materials and Engineering
Volume 47, Issue 3, March 2018
Online English edition of the Chinese language journal

Available online at www.sciencedirect.com

Cite this article as: Rare Metal Materials and Engineering, 2018, 47(3): 0773-0779.

ARTICLE

Influence of Hot Extrusion and Aging Treatment on the Properties of Biodegradable Mg-Zn-Y Alloy

Qiao Xueyan[1,2], **Yu Kun**[1,2], **Chen Liangjian**[3], **Dai Yilong**[1], **Xiao Tao**[4], **Deng Youwen**[4], **Yan Yang**[1]

[1] Central South University, Changsha 410083, China; [2] Yantai Nanshan University, Yantai, 265713, China; [3] Xiangya Third Hospital, Central South University, Changsha 410083, China; 4 Xiangya Second Hospital, Central South University, Changsha 410083, China

Abstract: Mg-6Zn-1Y (mass fraction, %) alloys were prepared for degradable biomaterials. The billets of the alloy were produced by powder metallurgy (PM) method and then hot extruded. The extruded samples were aged for 24 and 72 h at 150 °C. The microstructure and corrosion behavior of the experimental alloys were investigated. The microstructure observations indicate that the alloys contain α-Mg, MgZn, $MgZn_2$ and Mg_3YZn_6 (I-phase) phases. The hot extrusion process significantly refines the grains and leads to better mechanical properties with the value of compressive strength in the range of 365~399 MPa, and better corrosion resistance for the PM alloy shows higher hydrogen volume in the immersion test. Furthermore, due to more uniform corrosion behavior, the alloy aged for 72 h presents lower corrosion rate and corrosion current density in the immersion test and potentiodynamic polarization test, and higher resistance value (R_p) results from the electrochemical impedance spectroscopy (EIS), which means the alloy aged for 72 h exhibits better corrosion resistance than the other three alloys.

Key words: magnesium alloy; biomaterial; extrusion; aging; corrosion properties; mechanical properties

Magnesium and its alloys have attracted wide attention on biodegradable orthopaedic implants due to their excellent biodegradation and bone-like mechanical property[1,2]. The implants made by magnesium will degrade during the healing period of injured bone and need not to be removed in a secondary surgery. However, magnesium and its alloys show poor corrosion resistance, especially in solution containing chloride ion (Cl^-), which has greatly restricted their practical clinical application as implant materials. Many effective measures have been taken into consideration, such as alloying treatment and deformation processing[3]. Zn-containing and Y-containing Mg alloys like Mg-Zn alloys[4], and WE43[1,5] alloys have been studied a lot for their excellent corrosion resistance, good biocompatibility and suitable mechanical properties.

It has been reported that Zinc is one of the most abundant nutritionally essential and no-toxic elements in human body [6]. The addition of Zn facilitates the formation of a protective passive film on the surface of the magnesium alloy, which improves the corrosion resistance in the body fluid [7]. Besides, Zn can slow down the corrosion rate of magnesium alloys by elevating the corrosion potential in simulated body fluid (SBF) [4]. RE element yttrium (Y) can promote the formation of protective surface film and enhance the corrosion resistance of magnesium alloys [8]. The addition of Y in Mg-Zn alloy can induce the formation of ternary equilibrium Mg-Zn-Y phases which can restrain grain growth during dynamic recrystallization, and thus more refined grains are obtained during plastic deformation[9]. Although different binary or ternary phases are found in Mg-Zn-Y alloys due to different ratios of Zn/Y, the strength and creep resistance of the alloys are largely determined by

---

Received date: March 15, 2017
Foundation item: National Natural Science Foundation of China (81472058); Fundamental Research Funds for the Central Universities of Central South University (621020094); Shandong Province Project of Outstanding Subject Talent Group; the Innovation Project of Graduate Students, Central South University, China (2014zzts172)

Corresponding author: Yu Kun, Professor, Ph. D., School of Materials Science and Engineering, Central South University, Changsha 410083, E-mail: yukun2010@csu.edu.cn

the Mg_3YZn_6 phase (I-phase) in the previous work[10]. However, Liu[11] reported that too high Y content will cause severe micro-galvanic corrosion because of the large amount of Y-containing intermetallic compounds. Therefore, the low content Y is a reasonable choice.

Powder metallurgy (PM) is a promising method to prepare alloys and it can alter their properties by changing the ratio of element powder. Studies on magnesium matrix composite have been taken on this preparation method [12]. Moreover, previous studies reported that lower extrusion temperature and lower extrusion ration resulted in finer grains and better corrosion resistance [13-15]. Besides, it can obtain better distribution of I-phase in the Mg matrix using thermo-mechanical processes[16]. Therefore, Mg-6Zn-1Y alloys in the present paper were prepared by powder metallurgy, hot extrusion and heat treatment. The microstructure and corrosion behavior of the alloys in different states (PM sintered state, as-extruded state and as-aged state) were investigated in Ringer's solution to evaluate their biodegradability.

1 Experiment

The experimental alloys have the composition of 6%Zn, 1%Y and the rest of it is Mg. The samples were prepared by powder metallurgy method sintered in a vacuum furnace at 620~640 °C for 2 h under argon gas protection. The sintered billets (named PM) were pre-heated at 300 °C for 2 h and then hot extruded into Φ20 mm rods with an extrusion ratio of 9:1. The extruded rods (named EX) were aged at 150 °C for 24 h (named A1) and 72 h (named A2).

The experimental samples cut from the four alloys were 10 mm×10 mm×5 mm in size and were all ground with SiC abrasive paper up to 2000 grit and polished by absolute ethanol subsequently.

The microstructures of the PM, EX, A1 and A2 specimens were observed by an OLYMPUS optical microscope (OM) and a JSM-7800F scanning electron microscope (SEM) with an energy dispersive spectroscope (EDS). The microstructures of EX, A1 and A2 samples were observed from extrusion direction (RD) of the extruded rods. The phase analysis of the four state alloys were conducted using D/MAX-2500X X-ray diffraction (XRD). The specimens were etched by the solution: ethanol 100 mL, picric acid 5 g, acetic acid 5 mL and distilled water 10 mL.

Compressive test was carried out at room temperature by a MTS810 machine with a compression speed 1 mm/min. The samples were machined into cylinders with 10 mm in diameter and 20 mm in height. The results are from the average value of three repeat tests.

Immersion tests were carried out in (37±0.5) °C Ringer's solution, which contains sodium 8.6 g/L, potassium chloride 0.3 g/L, calcium chloride 0.33 g/L and the remaining composition is distilled water. The evolved hydrogen value and pH value were recorded every 4 h during the 72 h immersion. After 24 and 72 h immersion time, the microstructures of the specimens were characterized by SEM with EDS and XRD. The corrosion products formed on the surface were removed using a boiling 20% chromic acid + 1% $AgNO_3$ solution and cleaned by ultrasonic in absolute ethanol.

The electrochemical tests were carried out using CHI660D electrochemical system. The standard three-electrode cell system was used with a saturated calomel electrode (SCE) as the reference electrode and a platinum plate as the counter one at (37±1) °C in the Ringer's solution. The potentiodynamic polarization test was performed at a scanning rate of 1 mV/s. Electrochemical impedance spectra (EIS) were measured with the frequency range between 100 kHz and 10 mHz using the AC potential amplitude at 10 mV. The results are from the average value of three repeat tests.

2 Results and Discussion

2.1 Microstructures and mechanical properties of the four alloys

The microstructures of the PM, EX, A1 and A2 alloys are shown in Fig.1 and Fig.2. The average particle size of the PM alloy is about 7~33 μm (Fig.1a). Compared to the coarse particles resulting from the powder metallurgy method, the microstructures of the as-extruded alloys are refined with smaller grain size, as shown in Fig.1b~1d. These fine equiaxed grains are significantly refined by dynamic recrystallization during hot deformation. The average grain sizes of the A1 and A2 alloy are similar to each other but both larger than that of the EX alloy due to the aging treatment, which is shown in Fig.1c~1d. As shown in Fig.2a, the addition of alloying elements (Zn and Y) leads to formation of secondary phases. These phases distribute randomly in the α-Mg matrix with different sizes. The large particles are crushed into strip-like secondary phases after hot extrusion and distributed along ED (Fig.1b~1d). The amount of strip-like secondary phase increases due to aging treatment as is shown in Fig.2b and Fig.2c, and changes little with the increase of aging time (Fig.2c and Fig.2d). To further determine the phase composition, the four Mg-6Zn-1Y alloys were analyzed by XRD (Fig.3). The results show that the main phases are α-Mg, MgZn and I-phase (Mg_3YZn_6), while other phase such as $MgZn_2$ phase is also detected. It can be seen that $MgZn_2$ phase and I-phase are much more easier to be detected in the A1 and A2 alloys than those in the EX and PM alloys. Moreover, from the insert in Fig.2d, there are small precipitated phases distributed along ED in the A2 alloy. Combined with the results in XRD patterns, it can be deduced that those phases are $MgZn_2$ and I-phase.

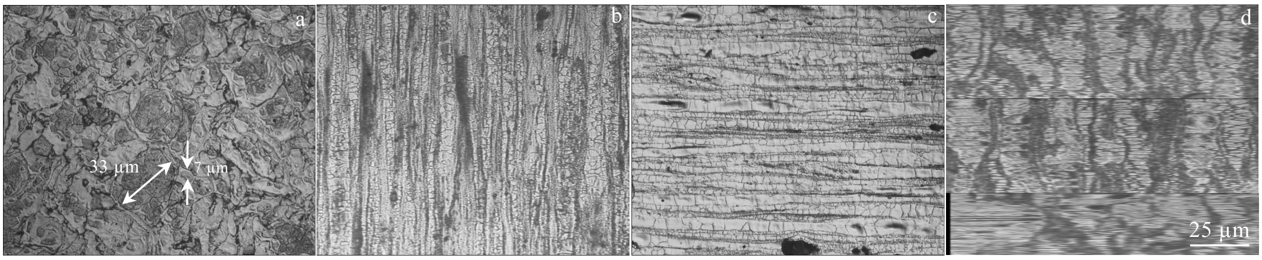

Fig.1 Optical micrographs of the four Mg-6Zn-1Y magnesium alloys: (a) PM, (b) EX, (c) A1, and (d) A2

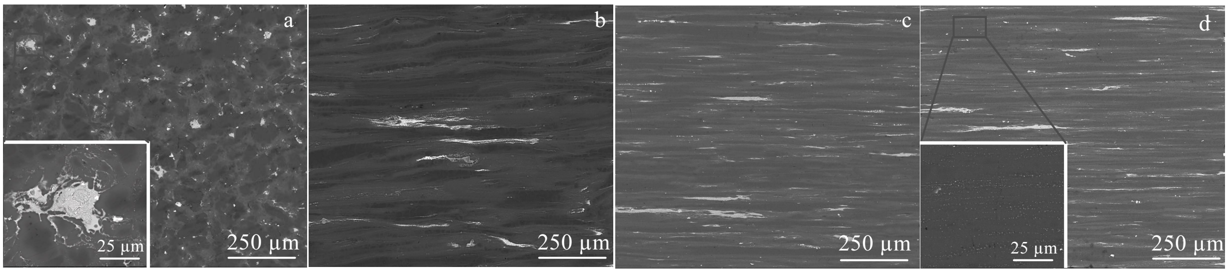

Fig.2 SEM images of the four Mg-6Zn-1Y alloys: (a) PM, (b) EX, (c) A1, and (d) A2

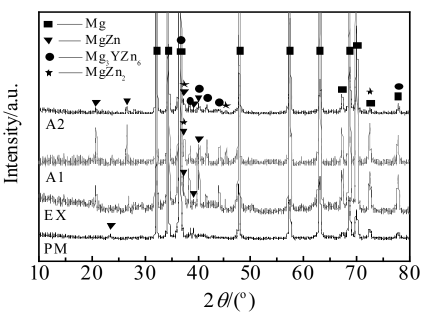

Fig.3 XRD patterns of the Mg-Zn-Y alloys

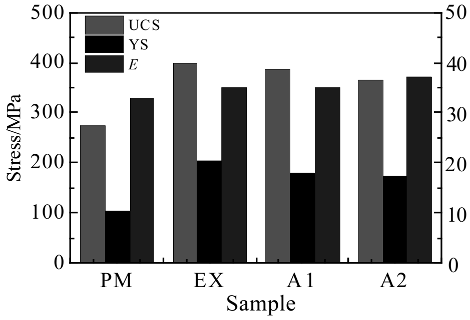

Fig.4 Mechanical properties of the four Mg-6Zn-1Y alloys

The mechanical properties including ultimate compression strength (UCS), yield strength (YS) and the modulus (*E*) of the four Mg-6Zn-1Y alloys at room temperature are displayed in Fig.4. The PM alloy has the lowest UCS (274 MPa) and YS (103 MPa), which is due to the large particles and coarse microstructure. The mechanical properties of the alloys are significantly enhanced after hot extrusion and the ultimate compression strength and yield strength are in the range of 365~399 MPa and 174~203 MPa. This is probably due to the refined microstructure which can be explained via the Hall-Petch equation. Besides, the elimination of the defects in the PM alloys also contributes to the good mechanical properties. The strength of the EX alloy is higher than that of the A1 and A2 alloys, which may result from the recovery during the low temperature aging treatment.

Moreover, the modulus of the four alloys are in the range of 33~37 GPa, which is close to the modulus of the natural bone (5~23 GPa). The results show that Mg-6Zn-1Y alloys exhibit good mechanical properties as medical metallic implants.

2.2 In *vitro* degradation performance

2.2.1 Immersion tests of experimental alloys in Ringer's solution

Fig.5 shows the change of hydrogen evolution volume (H_2^{evo}) and pH value of the solution for the four alloys with the increase of immersion time. During the 72 h immersion test, the H_2^{evo} of the PM alloy is higher than those of the other three alloys, indicating that hot extrusion can improve the corrosion resistance, as is reported by Birbilis[17]. Besides, the corrosion rates of the A1 and A2 alloys are slower than that of the EX alloy, which can be deduced that aging treatment may have a positive influence on slowing down the corrosion rate of magnesium alloy. Though the

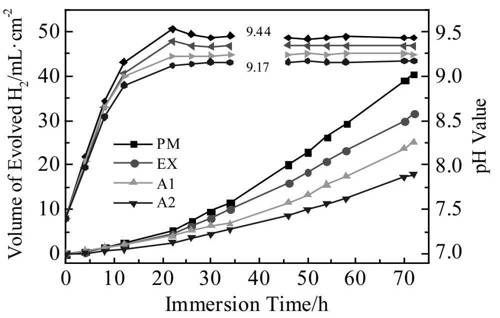

Fig.5 Hydrogen evolution volume and pH value of Mg-6Zn-1Y alloy immersed in Ringer's solution for 3 d

number of second phases in the A2 alloy is close to that of A1 alloy, the distribution of second phase for A1 and A2 alloy is different: for the A1 alloy, the second phase is dispersed locally with large size, while for the A2 alloy, there are a large number of small size secondary phases, especially I-phase, dispersed uniformly in the α-Mg matrix (Fig.3). F. Shi [18] has reported that a lot of fine and dispersed I-phases in the α-Mg matrix can slow down the corrosion rate of Mg alloys. Besides, as the grains are refined in the A1 and A2 alloys, with many small size phases distributed continuously in the α-Mg matrix of the A2 alloy and the distance between each secondary particles in the α-Mg matrix smaller than that of the A1 alloy, the corrosion reaction between the α-Mg matrix and the secondary phases will be impeded by the formation of the corrosion product and thus slow down the corrosion rate of the A2 alloy to a certain extent [19].

The release of hydrogen results in the increase of OH^- concentration of the solution. The pH variation over the 72 h of the immersion test is shown in Fig.5. During the first 20 h, the pH value of the solution increases rapidly with immersion time. All the alloys come to the dynamic state after 30 h immersion, as the formation rate and the dissolution rate of the magnesium hydroxide and other products have reached a balance state. At the end of the 72 h immersion tests, the pH is 9.45 for the PM alloy, 9.35 for the EX alloy, 9.24 for the A1 alloy and 9.16 for the A2 alloy.

To investigate the corrosion progress of the Mg-6Zn-1Y alloys, the A1 and A2 alloys with better corrosion resistance are chosen, and the corrosion morphologies with corrosion product of the A1 and A2 alloys after immersed for 24 and 72 h are presented in Fig.6a~6d. And Fig.6e~6f represent the corrosion morphologies without corrosion product after being immersed for 72 h. With the increasing of immersion time, more white corrosion products are formed on the surface of the both alloys. The XRD analysis of the corrosion product of the two alloys is shown in Fig.7, and the results reveal that the main composition of the white products is $Mg(OH)_2$, while some Y-containing oxides such as Y_2O_3 and $Y(OH)_3$ are found in the corrosion product of the A2 alloy. In Fig.6e~6f, pit corrosion has been seen in both alloys, but the A2 alloy exhibits more uniform corrosion morphology than the A1 alloy. The secondary phases in the α-Mg matrix will lead to micro galvanic reaction when exposed to Ringer's solution and the α-Mg matrix will dissolute for acting as the anode phase. For the A2 alloy, there are a large number of small secondary

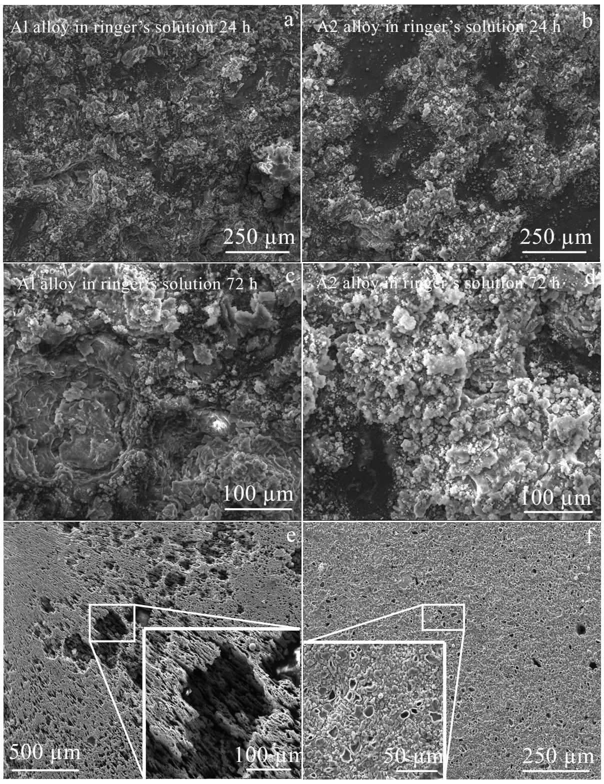

Fig.6 Surface morphologies of Mg-6Zn-1Y alloy: (a~d) A1 and A2 alloys before removing the corrosion products; (e~f) A1 and A2 alloys after removing the corrosion products

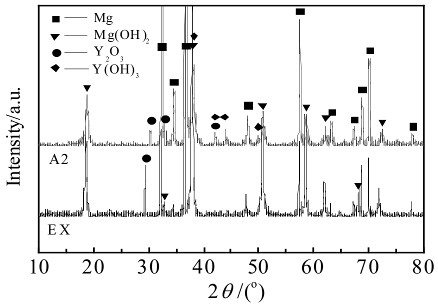

Fig.7 XRD patterns of the corrosion products

phases in the α-Mg matrix. Once the α-Mg matrix around the secondary phases dissolute, the secondary phases will fall off from the matrix leaving small pits on the surface of the alloy. Meanwhile, these pits will be filled with corrosion products formed in the reaction and thus slow down the corrosion rate. However, for the A1 alloy, there are not enough corrosion products to fill the deeper and larger pits in α-Mg matrix compared to the A2 alloy when secondary phases fall off from the surface. Hence, the pits are exposed to the Ringer's solution and the secondary phases inside the pits start to react with the fresh α-Mg matrix, which accelerate the corrosion rate of the A1 alloy. Therefore, localized corrosion has a bad effect for biodegradable alloys, for it may lead a division of alloys and destroy the mechanical property when exposed in body fluid even though the corrosion rate is low [20]. On the contrary, uniform biodegradation will prevent this large size collapse of the implant alloy. Therefore, the A2 alloy shows good corrosion resistance during the immersion test due to more uniform corrosion behavior.

Magnesium is an active metal that will react with water when immersed in Ringer's solution. During the reaction, the hydrogen gas is released from the solution and corrosion products are formed on the surface of alloy. The whole reaction of this corrosion process can be described as follows:

$$Mg \rightarrow Mg^{2+} + 2e^{-} \text{(anodic reaction)} \quad (1)$$

$$2H_2O + 2e^{-} \rightarrow H_2 + 2OH^{-} \text{ (cathodic reaction)} \quad (2)$$

$$Mg + 2H_2O \rightarrow Mg(OH)_2 + H_2\uparrow \text{ (total reaction)} \quad (3)$$

According to the reactions, $Mg(OH)_2$ is deposited on the surface of magnesium alloys and a protective film is formed to prevent further corrosion. However, the Cl^- in the Ringer's solution will accelerate the corrosion rate of magnesium alloys for the reason that $Mg(OH)_2$ can be transformed into more soluble $MgCl_2$[21], due to the following reaction:

$$Mg(OH)_2 + 2Cl^{-} \rightarrow MgCl_2 + 2OH^{-} \quad (4)$$

Then, the weakest areas of passive films will preferentially act as anodic sites and cause the localized corrosion [22], just like the severely localized corrosion in Fig.6e. Furthermore, Y element is detected in the corrosion products according to Fig.7. It exists as yttrium-containing oxide film and it can be deduced that following reactions [23] have occurred:

$$4Y + 3O_2 \rightarrow 2Y_2O_3 \quad (5)$$

$$Y_2O_3 + 3H_2O \rightarrow 2Y(OH)_3 \quad (6)$$

The addition of Y can increase the corrosion resistance for the presence of Y_2O_3 layer on the surface [24]. This is because that compared to the α-Mg = 0.81 (density of oxide film for Mg) [25], the value for Y is much bigger (αY>1), leading to a more compact Y_2O_3 oxide film. Besides, the increased I-phases can act as effective barriers to suppress the growth of pits as is reported by D. K. Xu et al [23]. Therefore, the fine dispersed small size Y contained I-phases are beneficial for preventing the A2 alloy from severe pit corrosion in Fig.6, and the film formed on the surface of the A2 alloy is more protective, which both lead to better corrosion resistance.

2.2.2 Electrochemical measurements of experimental alloys

To investigate the corrosion behavior during the 72 h immersion test, the polarization curves of the four alloys immersed in Ringer's solution for 1, 12, 24, 48 and 72 h are shown in Fig.8. The variation of corrosion potential (E_{corr}) and corrosion current density (J_{corr}) are presented in Fig.9.

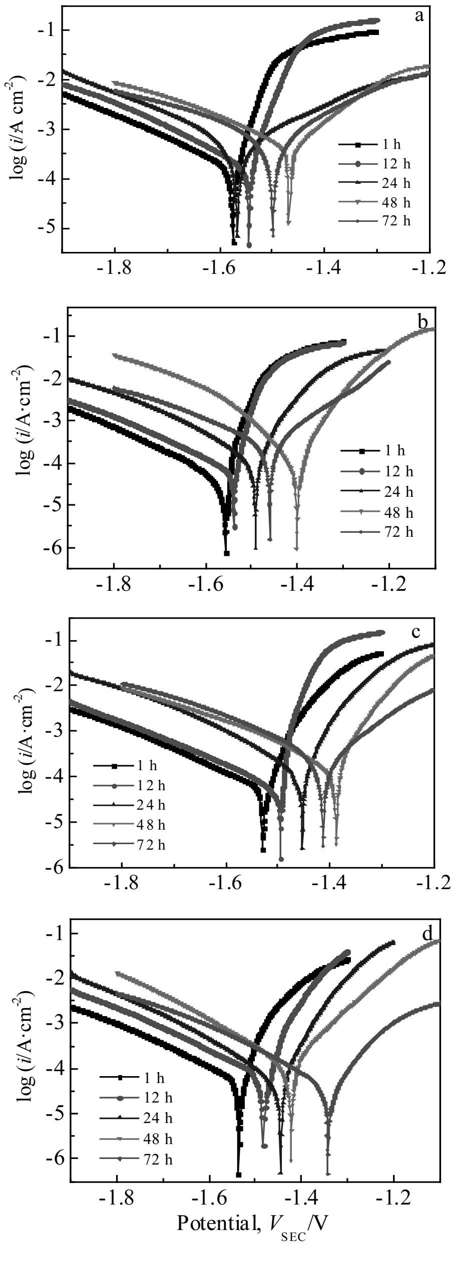

Fig.8 Potentiodynamic polarization curves for the alloys immersed in Ringer's solution for different time: (a) PM, (b) EX, (c) A1, and (d) A2

All the potentiodynamic polarization curves of the four alloys are very similar and the values of initial E_{corr} are close. Fig.9 shows that the E_{corr} of the PM alloy during the 72 h immersion reaches its noblest value of –1.469 V at 48h with J_{corr} reaching the top at the same time. The J_{corr} of the PM alloy is much higher than that of the other three alloys in every time interval, which indicates its poor corrosion resistance. The J_{corr} of the EX and A1 alloy are close during the 72 h immersion and are much lower than that of the PM alloy, which suggests that hot extrusion can slow down the corrosion rate. The A2 alloy exhibits a steady increasing in E_{corr} during the 72 immersion and the J_{corr} changes little in the range of 39.81~79.43 μA/cm^2, which indicates a steady corrode in Ringer's solution. As the J_{corr} value has a relationship with the corrosion rate, the A2 alloy with the lowest J_{corr} value shows its best corrosion resistance among the four alloys.

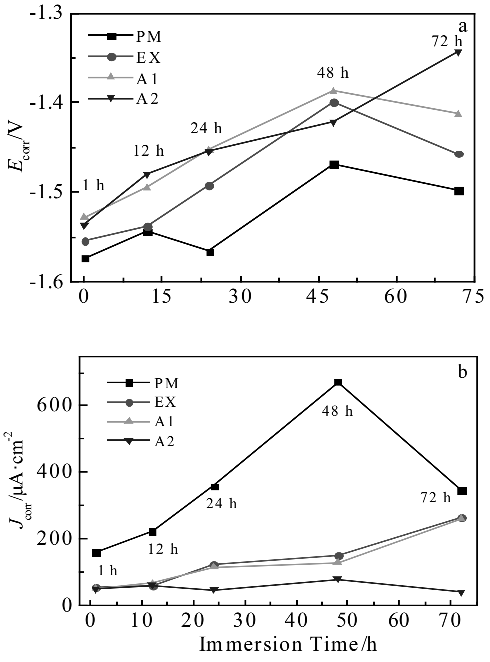

Fig.9 E_{corr} (a) and J_{corr} (b) of the four Mg-6Zn-1Y alloys

3 Conclusions

1) The grains of the EX, A1 and A2 alloys are refined due to dynamic recrystallization occurring during the hot extrusion. Strip second-phases can be observed after extrusion and small phases precipitate in matrix α-Mg after 72 h aging. The second-phases are proved to be MgZn, $MgZn_2$ and I-phase.

2) The mechanical properties of the alloys are enhanced by the hot extrusion and the values of compressive strength of the PM, EX, A1 and A2 alloys are 274, 365, 385 and 399 MPa, respectively. The modulus of the four alloys are in the range of 33~37 GPa, which is close to that of the natural bone.

3) The results of immersion tests show that the A2 alloy exhibits the slowest corrosion rate and the conclusion derived from the result of potentiodynamic polarization curves are the same as that from immersion tests. Therefore, the A2 alloy exhibits better corrosion resistance than the other three alloys.

4) The corrosion resistance of the EX alloy, A1 alloy and A2 alloy are much better than the PM alloy, due to the fine grains obtained by hot-extrusion. Aging time also influences the corrosion resistance of Mg-6Zn-1Y alloy, attributed to the alternative distribution and effect of varying second particles.

5) Pit corrosion occurs during the corrosion process and the A2 alloy shows better corrosion resistance than the EX alloy after 72 h immersion due to a more protective surface film and uniform corrosion behavior.

References

1 Witte F, Kaese V, Haferkamp H *et al. Biomaterials*[J], 2005, 26 (17): 3557

2 Krause A, Von Der Höh N, Bormann D *et al. Journal of Material Science*[J], 2010, 45 (3): 624

3 Wang H, Estrin Y, Zúberová. *Materials Letters*[J], 2008, 62 (16): 2476

4 Zhang S X, Zhang X N, Zhao C L *et al. Acta Biomaterialia*[J], 2010, 6 (2): 626

5 Gu X N, Zheng Y F *et al. Acta Biomaterialia*[J], 2010, 7 (4): 4605

6 Tapiero H, Tew K D. *Biomedicine and Pharmacotherapy*[J], 2003, 57(9): 399

7 Song G L, Atrens A. *Advanced Engineering Materials*[J], 1999, 1 (1): 11

8 Zeng R C, Chen J, Dietzel W *et al. Transactions of Nonferrous Metals Society of China*[J], 2007, 17 (S1): 166

9 Wang J F, Gao S, Song P F. *Journal of Alloys and Compounds*[J], 2011, 509(34): 8567

10 Wan D Q, Yang G C, Lin L *et al. Materials Letters*[J] , 2008, 62 (10-11): 1711

11 Liu M, Schmutz P, Uggowitzer P J *et al. Corrosion Science*[J], 2010, 52 (11): 3687

12 Dai Y L, Yu K, Chen L J *et al. Journal of Central South University*[J], 2015, 22 (3): 829

13 Zhang X B, Yuan G Y, Mao L *et al. Journal of the Mechanical Behavior of Biomedical Materials*[J], 2012, 7(1): 77

14 Zhang X B, Yuan G Y, Niu J L *et al. Journal of the Mechanical Behavior of Biomedical Materials*[J], 2012, 9(3): 153

15 Orlov D, Ralston K D, Birbilis N *et al. Acta Materialia*[J], 2011, 59 (15) : 6176

16 Asgharzadeh H, Yoon E Y, Chae H J *et al. Journal of Alloys*

and Compounds[J], 2014, 586 (S1): S95

17 Birbilis N, Ralston K D, Virtanen S. *Corrosion Engineering Science & Technology*[J], 2010, 45 (3): 224

18 Shi F, Yu Y C, Guo X F. *Transactions of Nonferrous Metals Society of China*[J], 2009, 19(5): 1093

19 Atrens A, Ming L. *Materials Science and Engineering B*[J], 2011, 176(20): 1609

20 Shi Z M, Liu M, Atrens A. *Corrosion Science*[J], 2010, 52(2): 579

21 Li Z J, Gu X N, Lou S Q, Zheng Y F. *Biomaterials*[J], 2008, 29(10): 1329

22 Song Y W, Shan D Y, Chen R S. *Corrosion Science*[J], 2009, 51 (5): 1087

23 Xu D K, Yin M Z, Han E H. *Scripta Materialia*[J], 2014, 71(3): 21

24 Liu M, Schmutz P, Uggowitzer P J *et al. Corrosion Science*[J], 2010, 52(11): 3687

25 Li G Q, Wu G H, Fan Y *et al. Foundry Technology*[J], 2006, 27(1): 79 (in Chinese)

热挤压和时效处理对生物可降解 Mg-Zn-Y 合金性能的影响

乔雪岩[1,2]，余　琨[1,2]，陈良建[3]，戴翌龙[1]，肖　涛[4]，邓幼文[4]，颜　阳[1]

(1. 中南大学，湖南 长沙 410083)

(2. 烟台南山学院, 山东 烟台 265713)

(3. 中南大学 湘雅三医院，湖南 长沙 410083)

(4. 中南大学 湘雅二医院，湖南 长沙 410083)

摘　要：采用粉末冶金法制备了 Mg-6%Zn-1%Y 生物医用镁合金并进行了热挤压变形处理。挤压后的样品在 150 ℃下分别时效 24 和 72 h。对实验用合金的显微组织和腐蚀行为进行了研究。显微组织结果表明，合金包含 α-Mg、MgZn、$MgZn_2$ 和 Mg_3YZn_6（I 相）。热挤压工艺显著细化晶粒并提高了合金的力学性能和耐腐蚀性能。其中热挤压后合金的压缩强度在 365~399 MPa 之间，且浸泡实验中的析氢量低于烧结态合金。另外，由于更均匀的腐蚀行为，时效 72 h 的合金分别在浸泡实验和动电位极化实验中显示出更低的腐蚀速率和腐蚀电流密度，并在电化学阻抗谱(EIS)中获得了较高的电阻值(R_p)。结果表明，时效 72 h 合金较其他 3 种合金具有更优异的腐蚀性能。

关键词：镁合金；生物材料；挤压；时效；腐蚀性能；力学性能

作者简介：乔雪岩，女，1990 年生，硕士，中南大学材料科学与工程学院，湖南 长沙 410083，电话：0731-88879341，E-mail: qxy_langya@163.com